Los Alamos National Laboratory is operated by the University of California for the United States Department of Energy under contract W-7405-ENG-36

LA-UR--91-1693

DE91 013687

TITLE STRESS FIELDS GENERATED BY KINETIC ENERGY PROJECTILE INTERACTION WITH CERAMIC TARGETS

AUTHOR(S) M. W. Burkett
D. A. Rabern

SUBMITTED TO APS 1991 Topical Conference, Williamsburg, VA, ~~June~~ July 17-20, 1991

DISCLAIMER

Los Alamos National Laboratory
Los Alamos, New Mexico 87545

STRESS FIELDS GENERATED BY KINETIC ENERGY PROJECTILE INTERACTION WITH CERAMIC TARGETS

Michael W. BURKETT and Donald A. RABERN

Two-dimensional axisymmetric calculations were performed with the Eulerian hydrocode MESA2D and the Lagrangian structural analysis code PRONTO2D. The calculated stress distributions were compared shortly after impact and found to be similar in magnitude and profile. For certain geometric configurations, the interaction of the kinetic energy penetrators with the ceramic targets produce high compressive principal stresses as well as, significant tensile principal stresses ahead of the projectile/ceramic interface. The principal tensile stresses fracture the ceramic ahead of the penetrator. The crack trajectories measured from a recovered ceramic target were compared with crack trajectory estimates based upon MESA2D principal stress states within the tile. The fracture process degrades the ceramic and allows the projectile to penetrate a fractured ceramic media.

1. INTRODUCTION

Ceramics have been considered candidate armor materials because of certain mechanical properties and observed performance during ballistic testing. Low densities, high shear moduli, and compressive strengths are a few of the material properties that make ceramics desirable armors especially against kinetic energy penetrators. However, low tensile strengths often prevent ceramics from achieving their ultimate potential as an armor material.

In recent years, the interest in understanding the behavior of ceramics during dynamic loading/deformation has increased. Several institutions have performed independent assessments of various ceramics' ballistic performance.[1-3] Also, characterization of ceramics under different loading conditions has been investigated.[4,5] A complete explanation of the behavior of ceramics during dynamic loading and deformation events has not yet been formulated.

Research that combines experimental and analytical efforts can be employed to obtain additional insights into ceramic armor behavior. In our study, we investigated the response of a candidate armor material to an impact and partial penetration by a high-density long-rod penetrator (LRP) experimentally and analytically. We recovered the ceramic tile from a ballistic test in which the LRP engaged the target and penetrated a few rod diameters. The recovered tile was stabilized with epoxy and sectioned to reveal the extent of damage and the crack orientations. The principal stress distribution and orientation was calculated with MESA2D[6] for comparison with the observed crack orientation and extent of damage found in the sectioned tile. Also, we compared the general stress field distribution calculated with MESA2D (an Eulerian hydrocode) with the stress distribution calculated with PRONTO2D[7] (a Lagrangian structural analysis code) to ensure the validity of the hydrocode stress field.

2. BALLISTIC IMPACT EXPERIMENT

2.1. Impact Conditions

A ballistic impact experiment was performed to investigate the response of an aluminum oxide (Al_2O_3) ceramic when engaged by a high-density LRP. The ceramic was manufactured by Coors and was approximately 85 wt% alumina (AD85). The tile was cylindrical: 9.84 cm (3.875-in.) in diameter and 8.89 cm (3.5-in.) thick. Steel confinement was used to support all surfaces of the tile. A 0.64 cm (0.25-in.)-thick 4340 steel (Rc 42) cover plate was positioned on the front surface while a 2.54-cm (1.0-in.)-thick 4340 back plate was used to support the ceramics' rear surface. A mild steel (AISI 1010) cylinder was used to provide lateral stiffness. Belzona (an epoxy loaded with ceramic particles) was used to ensure a tight fit within the confinement. Figure 1 shows the cross section of the target. A high-density penetrator with an L/D ratio of approximately 2 was accelerated to the 0.13 cm/μs impact velocity by a smooth-bore powder gun. Dynamic radiography was not used to record the interaction because we were primarily interested in the fracture response of the tile, and not in its ballistic performance.

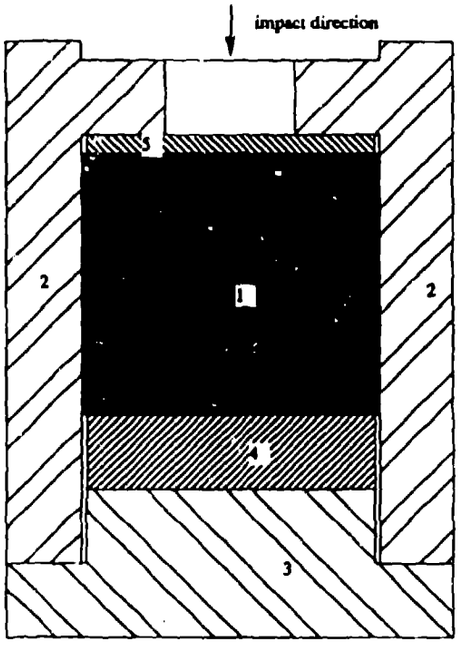

1 - Ceramic Tile
2 - Mild Steel Lateral Confinement
3 - Mild Steel Canister Cap
4 - 4340, Rc 40-42 Backing Plate
5 - 4340, Rc 40-42 Cover Plate

Fig. 1 Ceramic target cross section.

2.2. Posttest Target Inspection

Following the test, the target was recovered and stabilized under vacuum with an epoxy. After stabilization, the lateral confinement was removed, and vertical and horizontal sections were made. Figure 2 shows the vertical section of the posttest tile. The section shows no signs of a residual penetrator in the crater formed by the impact. A network of cracks are concentrated around the impact crater. Other cracks (Hertzian cone cracks) emminate from the impact point at angled trajectories ranging from 0 to 60° from the vertical and are clearly visible in this section. The horizontal section shows radial and circumferential cracks surrounding the impact region.

The crack profiles found in our target are similar to profiles found in brittle specimens following static indentation tests.[8,9] For static or quasi-static indentation tests, the stress field produced in the elastic specimen beneath the indenter determines the ensuing fracture configuration observed in the specimen following the test.[10] Cracks at any point within the specimen tend to propogate along trajectories of lesser principal stresses (obtained from the elastic stress field prior to fracture) and maintain orthogonality to the major principal tensile component direction.[11] Since our ballistic test produced fracture patterns similar to those found in the indentation tests, we wanted to determine whether the dynamic stress field generated by the LRP striking the target was an indicator of the crack paths observed in the recovered ceramic tile.

3. ANALYSES OF BALLISTIC IMPACT EXPERIMENT

3.1. Modeling Assumptions

We simulated the ballistic impact experiment with the MESA2D hydrocode. We assumed that the responses of the LRP, cover plate, lateral confinement, and backup plate were elastic-perfectly-plastic. The response of the AD85 was assumed to be elastic. The yield strength of the AD85 was assumed to be 0.044 Mbar (4.4 GPa). No attempts were made to simulate the propogation of cracks by degrading elastic material properties or yield strength. We assumed that the impact could be simulated in axisymmetric geometry with a constant zone size of 0.077 cm.

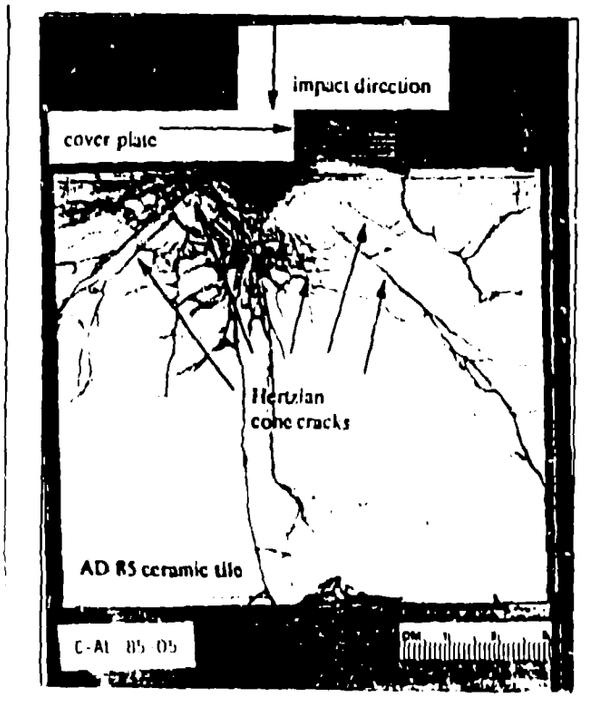

Fig. 2 Posttest stabilized ceramic tile.

3.2. Stress Distributions

Contour plots that show the distribution of axial, radial, shear, and hoop stress generated by the penetrator shortly after impact indicate a complex state of stress in the ceramic. At 5 μs, the LRP has not fully penetrated the cover plate, but has induced significant compressive and tensile stresses in the ceramic in the vicinity of the impact point. We decided to investigate the state of stress in the ceramic at the earliest time when the tensile stresses were of sufficient magnitude to induce fracture. During a dynamic fracture experiment, the stress field is continually changing to reflect the introduction of fracture surfaces within the material. Since the code has no models that simulate fracture, we were primarily interested in analyzing the stress state at a time when the stress levels were of sufficient magnitude to initiate fracture. The code predicts compressive axial and shear stresses that are present in the tile. The magnitude of the axial stresses are near the assumed yield strength of the ceramic, while the maximum shear stress was slightly above 0.0125 Mbar. The radial and hoop stress fields show compressive stresses in the tile directly beneath the cover plate and tensile stresses approximately 1 cm below the tile/cover plate interface. Tensile stress that exceeded the tensile strength of the ceramic by at least 0.008 Mbar (0.8 GPa) were calculated for the radial and hoop stresses. Tensile stresses of 0.007 Mbar (0.7 GPa) were found in the ceramic. The tensile strength of the AD85 was assumed to be 0.0016 Mbar (0.16 GPa).

3.3. Principal Stress Directions and Crack Trajectories

The investigation of crack trajectories in the ceramic required that the magnitude and direction of the principal stress field in the tile be calculated. We obtained principal stress field distributions in the radial and axial plane of the tile by using the CCCP[12] hydrocode postprocessor. Stress contour plots indicate the magnitude of the principal stresses in this plane, but not their directional dependence. Estimates of the crack paths required that the plane upon which the tensile principal stresses act be calculated.

In order to show the combined effect of the principal stress magnitude and direction, the CCCP code was modified to provide stress vector plots. The length of the stress vector is proportional to the stress magnitude, while the vector orientation indicates the stress direction. Only tensile principal stress values exceeding 0.0016 Mbar (0.16 GPa) (maximum allowable tensile stress) were included to show the effect of direction. If the tensile principal stress value was less than 0.0016 Mbar (0.16 GPa), the data was not included.

Since cracks at any point within the ceramic will propogate orthogonal to the maximum principal stress component direction, we produced an orthogonal stress vector plot (vectors orthogonal to the maximum principal stress direction) to show estimates of crack trajectories. Figure 3 shows the distribution of the maximum principal stress in this plane on the right hand side of the figure (RHS), and the estimated crack trajectories (based upon principal stress magnitudes and directions) on the left hand side of the figure (LHS). The trajectories near the plane of symmetry (a radial position of zero) are zero degrees, and they gradually decrease to approximately 60 degrees as the radial position approaches 2.0 cm. The magnitude of the tensile principal stresses in the region shown in Fig. 3 ranged from 0.0016 to 0.0100 Mbar (0.16 to 1.0 GPa).

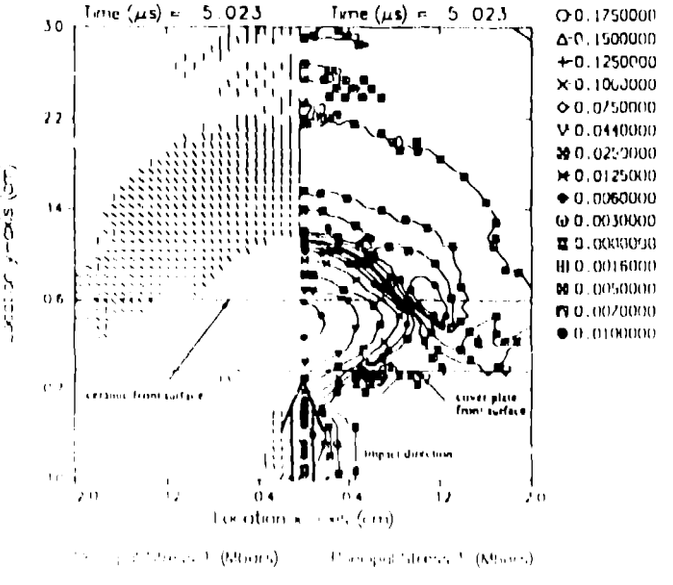

Fig. 3 Calculated maximum principal stress distribution (RHS) and estimated crack trajectories (LHS).

The estimated trajectories are within the range of the Hertzian cone crack paths and are located in the general region observed in the ceramic target. Careful inspection of the stabilized ceramic cross section shows that the magnitudes and orientations of the maximum principal stresses change as cracks are initiated. Some of the cracks begin propogating at a constant trajectory but are often terminated (by intersecting other cracks) or alter direction (as a result of the stress field reacting to the crack formation and propogation). The initiation of cracks alters the stress field, which directly influences the crack trajectory.

4. CONCLUSIONS

Two-dimensional axisymmetric calculations were performed with the Eulerian hydrocode MESA2D and the Lagrangian structural analysis code PRONTO2D. The calculated stress fields were compared at early times (prior to 10 μs) and found to be similar in magnitude and profile.

We investigated experimentally and analytically, the response of the AD85 alumina ceramic to an impact and partial penetration by a high-density LRP. The ceramic tile was recovered and stabilized with an epoxy and sectioned to reveal the extent of damage and crack orientation. The principal stress distribution and orientation were calculated with MESA2D. The hydrocode predicted principal tensile stresses of sufficient magnitude to induce fracture. The hydrocode estimates of crack trajectories and crack position (location of cracks within tile) are within the range of values for some of the cone cracks found in the sectioned tile. The estimated crack paths and locations were based upon the principal stress state within the ceramic.

ACKNOWLEDGMENTS

We would like to thank W. D. Birchler for his assistance with the analysis and his interpretation of the hydrocode calculations, and B. M. Wheat for making modifications to the CCCP graphics postprocessor that enabled us to interpret the hydrocode stress field more effectively.

The support provided by D. Marts and A. D. Rollett in stabilizing, sectioning, and photographing the fractured ceramic tile was greatly appreciated. Finally, we would like to thank L. L. Shelley and M. R. Martinez for assisting with the editing and preparation of this document.

REFERENCES

1. M. L. Alme and S. J. Bless, "Experiments to Determine the Ballistic Resistance of Confined Ceramics at Hypervelocity," Defense Advanced Projects Agency draft topical report (September 1988).

2. P. Woosley, S. Mariano, and D. Kokidko, "Alternative Test Methodology for Ballistic Performance Ranking of Armor Ceramics," presented at Fifth Annual TACOM Armor Coordinating Conference, Monterey, California (March 1989).

3. Z. Rosenberg, S. J. Bless, and N. S. Brar, "On the Influence of the Loss of Shear Strength on the Ballistic Performance of Brittle Solids," *International Journal of Impact Engineering* Vol. 9, No. 1, pp. 45-49 (1990).

4. M. E. Kipp and D. E Grady, "Shock Compression and Release in High-Strength Ceramics," Sandia National Laboratories report SAND89-1461 (July 1989).

5. D. E Grady, "Dynamic Material Properties of Armor Ceramics," Sandia National Laboratories report SAND91-0147 (March 1991).

6. T. Bennion and S. Clancy, "MESA2D Version 4," Los Alamos National Laboratory report LA-CP-90-323 (November 1990).

7. L. M. Taylor and D. P. Flanagan, "PRONTO2D - A Two-Dimensional Transient Solid Dynamic Program," Sandia National Laboratories report SAND86-0594 (March 1987).

8. B. R. Lawn and M. V. Swain, "Microfracture Beneath Point Indentations in Brittle Solids," *Journal of Materials Science* No. 10 pp. 113-122 (1975).

9. B. R. Lawn and M. V. Swain, "Review Indentation Fracture: Principles and Applications," *Journal of Materials Science* No. 10 pp. 1049-1081 (1975).

10. B. R. Lawn and M. V. Swain, "Review Indentation Fracture: Principles and Applications," *Journal of Materials Science* No. 10 pp. 1049-1081 (1975).

11. B. R. Lawn and M. V. Swain, "Review Indentation Fracture: Principles and Applications," *Journal of Materials Science* No. 10 pp. 1049-1081 (1975).

12. B. M. Wheat, "The Cell Coloring Computer Program User's Manual," Los Alamos National Laboratory report LA-10889-M (September 1987).